Numerical Modeling of Concrete-Filled FRP Tubes' Dynamic Behavior under Blast and Impact Loading

Yazan Qasrawi[1]; Pat J. Heffernan[2]; and Amir Fam, A.M.ASCE[3]

Abstract: A major difficulty of the analysis of and design for close-in blasts is the high variability of the blast shock waves and the complex interactions between these waves and structures. Close-in blasts also tend to be severe loads that may cause extensive damage to a structural member. If the member in question is a load bearing column, its destruction may lead to a catastrophic progressive collapse of the structure. Thus any improvement on the performance of columns under close-in blast loading is a valuable addition to knowledge. This paper outlines a numerical model built using commercially available software to predict the response of concrete filled fiber reinforced polymer (FRP) tubes (CFFTs) and regular round reinforced concrete members to impacts and close-in blasts and determine the factors influencing their response. The models were verified against drop weight impact test lab measurements and single degree of freedom blast analyses. A parametric study was conducted using the verified models to investigate the effects of diameter, reinforcement ratio, and size of the blast on the response of CFFTs. It was found that the peak displacement response was inversely proportional to all three parameters. The results of the parametric study were used to construct new pressure-impulse diagrams for experimentally tested CFFT specimens that reflect the increased capacity of such members to blast loading. **DOI: 10.1061/(ASCE)ST.1943-541X.0001370.** © 2015 American Society of Civil Engineers.

Author keywords: Concrete filled FRP tube (CFFT); Fiber-reinforced polymer (FRP) tube; Reinforced concrete; Hydrocode model; Close-in blast; Low velocity impact; Pressure-impulse diagrams; Analysis and computation.

Introduction

Close-in explosions, whether deliberate or accidental, are extreme loads that are notoriously difficult to predict and design against owing to the large number of interacting variables. Close-in explosions' effects on columns are of great importance because columns tend to be critical load bearing members whose collapse may initiate a progressive collapse of the structure. Thus, any improvement in the blast resistance of columns can potentially save lives and property.

Glass fibre reinforced polymer (GFRP) tubes, when used as stay-in-place forms, confine the concrete core and act as structural reinforcement ideally located at the perimeter making the concrete filled fiber-reinforced polymer (FRP) tube (CFFT) system well suited to blast resistant design.

The static performance of CFFTs has been investigated extensively, as in the study by Fam and Rizkalla (2002) of the flexural performance of CFFTs, the study by Cole and Fam (2006) of the enhancement of CFFTs by the introduction of internal steel and FRP reinforcement, the study by Fam and Mandal (2006) on prestressing the system, and the study of their behavior under combined axial and flexural loads by Flisak et al. (2001). Helmi et al. (2008) investigated the important problem of the fatigue behavior of GFRP

tubes, and ElGawady et al. (2010) and Zaghi et al. (2012) investigated the seismic behavior of CFFTs in two separate studies. CFFT behavior under blast loading, however, remained to be investigated.

Barker (2008) advocated the use of advanced analysis techniques, such as finite element analyses and computational fluid dynamics, to predict blast loads and structural response to assist in design. Luccioni et al. (2004) successfully simulated an explosion and the structural response of a building destroyed by a terrorist attack in the same model, capturing the resulting progressive collapse caused by the failure of the columns at the lower level. They concluded that such a detailed analysis was possible because of the advances in computers and the development of powerful numerical programs known as hydrocodes, and they proposed the use of such analyses in blast resistant design.

Malvar et al. (2007) found from surveying the literature that composites in the form of wrapping or near surface mounted plates increased the strength of existing members and helped prevent the collapse of load bearing members which may initiate a progressive collapse of the structure. Similarly, Buchan and Chen (2007) compared the results of experimental and numerical investigations of the effectiveness of retrofitting structures using FRP. They concluded that FRPs improved a structure's strength and stiffness, but that the behavior was not well understood owing to the complexity of the problem, and that most of the studies provided qualitative rather than quantitative results. They urged the development of design guidelines which are essential for the widespread use of FRP for blast resistant applications.

CFFT members promise to be optimal for blast-resistant construction; however, their dynamic behavior and the factors that influence their blast performance are not well understood.

This investigation numerically studied the performance of CFFTs under impact and close-in blasts, aiming to determine the factors that affect their response and to produce design limit recommendations.

The objectives of this investigation were:

1. To develop and verify a numerical model that captures the dynamic behavior of CFFTs under close-in blasts and impacts.

[1]Assistant Professor, Dept. of Civil Engineering, Royal Military College of Canada, P.O. Box 17000, Station Forces, Kingston, ON, Canada K7K 7B4 (corresponding author). E-mail: Yazan.Qasrawi@rmc.ca

[2]Vice-Principal, Research and Dean of Graduate Studies, Dept. of Civil Engineering, Royal Military College of Canada, P.O. Box 17000, Station Forces, Kingston, ON, Canada K7K 7B4. E-mail: Pat.Heffernan@rmc.ca

[3]Donald and Sarah Munro Chair Professor in Engineering and Applied Science, Dept. of Civil Engineering, Queen's Univ., Kingston, ON, Canada K7L 3N6.

Table 1. Experimental Specimen Details

Specimen designation	Testing method	Type	Reinforcement ratio (%)	Reinforcement configuration
CB4	50 kg of C4	RC	1.2	A
CB8-S	50 kg of C4	RC	2.4	C
CB8-L	100 kg of C4	RC	2.4	C
CI4	Impact	RC	1.2	A
CI8	Impact	RC	2.4	C
TB4	50 kg of C4	CFFT	1.2	B
TB8-S	50 kg of C4	CFFT	2.4	D
TB8-L	100 kg of C4	CFFT	2.4	D
TI4	Impact	CFFT	1.2	B
TI8	Impact	CFFT	2.4	D

2. To determine the effects of the diameter, internal steel reinforcement ratio, and the size of the blast on the behavior of CFFTs.
3. To make design guideline recommendations based on the numerical results.

This paper presents a detailed description of the development and validation of numerical models of CFFTs subjected to blast and impact loading. This description is followed by the development and results of a parametric study of the behavior of CFFTs subjected to close-in blast loading.

Description of Experimental Program and Specimens

Ten 4-m-long reinforced concrete specimens with a circular cross section were cast at the Royal Military College's structures laboratory. Of the 10 specimens, five were cast using conventional cardboard tube forms, and the other five were cast using GFRP tubes as stay-in-place forms. Six of the 10 specimens had a steel reinforcement ratio of 2.4%, corresponding to eight 10M longitudinal bars, and four had a steel reinforcement ratio of 1.2% corresponding to four 10M longitudinal bars. These steel reinforcement ratios

approximated the 1 and 2.5% minimum and maximum recommended blast design reinforcement ratios (Unified Facilities Criteria 2002; CSA 2004b) to ensure strength and ductility. All the specimens contained 6-mm continuous steel spiral shear reinforcement to prevent shear failure and maximize ductility. The spiral spacing was 0.1 m except within 0.2 m of the ends where it was reduced to 0.05 m to mitigate the effects of the support reactions. A summary of the specimens is presented in Table 1, and schematics of the specimens are presented in Fig. 1.

The specimens were tested under impact and close-in field blast. The full scale blast tests were conducted at the Canadian Forces Base in Petawawa with the assistance of 2 Combat Engineers Regiment (2 CER). The specimens were tested side by side to subject the test and control specimens to the same testing conditions. Two 0.15-m-long steel sleeves were used at the ends of the specimens to distribute the support loading and prevent local failure. The spherical explosive charges were supported on wooden frames 2 m above the top face of the specimens. The first pair of blast specimens, CB8-S and TB8-S, were tested under 50 kg of C4. The second pair of blast specimens, CB4 and TB4, were tested at the same explosive mass of 50 kg of C4 to facilitate comparison. Specimens CB8-L and TB8-L were tested under 100 kg of C4. The impact tests were conducted by dropping a 561 kg mass at the midspan of the specimens in a three-point bending simply supported configuration with a center-center span of 3.85 m. The specimens were restrained with additional top rollers at the supports to prevent rebounding. Similar to the blast tests, 0.15-m-long steel sleeves were placed at the supports and the loading point to distribute the forces and prevent local failures.

Numerical Modeling

Material Models

C4 and TNT Explosives
The ANSYS Autodyn material library's Jones-Wilkins-Lee (JWL) equation of state, which is predefined and already calibrated in
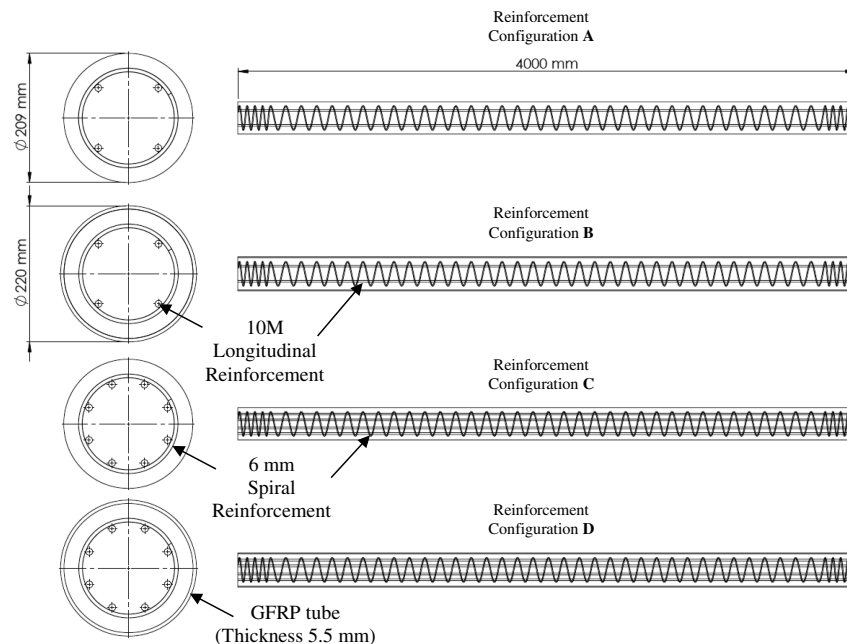

Fig. 1. Experimental specimens' reinforcement cage details

Table 2. *Autodyn* Input Parameters for Concrete, Steel, and GFRP Material Models

Material	Material model	Adjusted parameter	Value 10M rebar[a]	Comments
Reinforcing steel	Johnson Cook strength model	Yield stress (kPa)	4.30×10^5	Fitted to test data
		Hardening constant	2.57×10^5	Fitted to test data
		Hardening exponent	0.26	Fitted to test data
	Plastic strain failure	Plastic strain	0.1	Fitted to test data
	Plastic strain erosion	Erosion strain	0.1	Fitted to test data
Concrete	RHT concrete strength	Compressive strength (kPa)	3.4×10^4	Fitted to test data
	RHT concrete tensile stress failure	Principal tensile failure stress (kPa)	3.4×10^3	
		Crack softening fracture energy (J/m^2)	104.7	Calculated according to Bazant and Becq-Giraudon 2002
	Geometric strain erosion	Erosion strain	2.0	Program default
GFRP tube	General	Reference density $(g \cdot cm^{-3})$	1.938	Manufacturer's data
	Ortho equation of state	Young's modulus 11 (kPa)	1.01×10^7	Manufacturer's data
		Young's modulus 22 (kPa)	2.16×10^7	Manufacturer's data
		Poisson's ratio 12	0.35	Manufacturer's data
		Shear modulus 12 (kPa)	6.4×10^5	Manufacturer's data
	Von Mises strength	Shear modulus 12 (kPa)	6.4×10^5	Manufacturer's data
		Yield stress 11 (kPa)	4.83×10^4	—
	Material strain failure	Tensile failure strain 11	0.0184	Fitted to test data from Zakaib 2013
		Tensile failure strain 22	0.0184	Fitted to test data from Zakaib 2013
	Geometric strain erosion	Erosion strain	0.02	—

[a]The 6 mm spiral reinforcement had the same values as the 10M bars except for the Yield stress being 6.45×10^5 kPa and the Hardening constant being 2.38×10^5.

ANSYS Autodyn by fitting to experimental data for various types of explosives, was used to model the C4 and TNT explosives. It is common practice to simplify the JWL equation of state to that of an ideal gas at expansions of approximately 10 times the original volume, and this was utilized where applicable to speed up the calculations.

Air

ANSYS Autodyn's ideal gas equation of state, included in the standard material library (*ANSYS Autodyn 2005*), was used to model the air in the blast. The air's internal energy was set to 2.068×10^5 J to correspond to standard atmospheric pressure and temperature. The air material model had no strength or failure criteria.

Reinforcing Steel

Based on three tensile tests for each type of reinforcement, the 6-mm spirals had a tensile yield strength of 645 MPa and an ultimate strength of 713 MPa with a modulus of elasticity of 194 GPa. The 10M bars had a tensile yield strength of 430 MPa, and an ultimate strength of 577 MPa with a modulus of elasticity of 170 GPa. The linear equation of state (*ANSYS Autodyn 2005*) was used for the steel rebar. The Johnson and Cook constitutive model, built into *ANSYS Autodyn*, was used to capture the plastic flow of the reinforcing bars (Johnson and Cook 1983). The erosion strain was set to 0.1 to correspond to observations made during the tensile tests. The parameters that were adjusted in reinforcing steel's material models are presented in Table 2.

Concrete

The 28-day concrete compressive strength of the specimens, based on the mean of six cylinder tests, as per CSA A23.2-9 C (CSA 2004a), was 34 MPa. The P-alpha equation of state was used in *ANSYS Autodyn* to model the behavior of concrete before the pores collapsed and it was fully compacted. After the pores collapse and the concrete is fully compacted, *ANSYS Autodyn* reverts to the polynomial equation of state.

The Riedel, Hiermaier, and Thoma (RHT) model (Riedel et al. 1999), built into *ANSYS Autodyn*, was used to capture the dynamic

nonlinearity of concrete. The RHT model is an advanced plasticity model which captures the dynamic loading of brittle materials. The factorized formulation of the RHT fracture surface, where the increases or reductions in strength attributable to the strain rate and the stress state are calculated separately and then applied to the concrete strength as factors. The RHT model is setup in *ANSYS Autodyn* such that changing the concrete's compressive strength would automatically scale the remaining terms proportionately.

The concrete's tensile failure was defined in the model to be a maximum tensile stress that was 10% of the maximum compressive stress in addition to a crack softening option. Crack softening defines the tensile strain softening behavior, as the concrete loses its strength more or less gradually in tension after cracking. To fully define this behavior, three parameters were required, the maximum tensile stress, already defined, the shape of the descending branch, which is assumed to be linear in *ANSYS Autodyn*, and the area under the curve. The area under the curve represents the fracture energy, and it was estimated to be 104.7 J/m^2 based on the work of Bazant and Becq-Giraudon (2002). The adjusted parameters for the concrete material model are presented in Table 2.

GFRP Tube

The GFRP tube's mechanical properties, obtained from the manufacturer (Ameron International 1997, 2004), were a tensile modulus of 21.6 GPa and a Poisson's ratio of 0.45 in the circumferential direction, and a tensile strength of 48.3 MPa, at tensile modulus of 10.1 GPa, and a Poisson's ratio of 0.35 in the longitudinal direction, and a shear modulus of 6.4 GPa.

ANSYS Autodyn allowed the entry of the GFRP tube's material properties in terms of the engineering constants, which populated the compliance matrix. As the shell elements used to model the GFRP tube were two-dimensional elements, the through-thickness properties were omitted to achieve a plane stress situation. The Von Mises constitutive model was used to capture the GFRP tube's nonlinearity. Three coupons from a GFRP tube from the same manufacturer and with the same laminate structure were tested by Zakaib (2013) for another project. The coupon tests gave an average strength of 53 MPa, which was 9.7% higher than the value provided

by the manufacturer. The coupon tests also provided a rupture strain of 0.0184 for the tube. The parameters used in the GFRP tube's material model are presented in Table 2.

Verification Models

Model Descriptions

Because of inadequate measurements resulting from instrumentation failures during blast testing, the more detailed results of the impact tests and SDOF predications of the blast tests were used to validate the *ANSYS Autodyn* numerical model.

ANSYS Autodyn's sophisticated remapping capabilities were used to speed up the modeling time. The blast wave was initially modeled using a two-dimensional (2D) axisymmetrical model from the explosion out to 1.975 m, which was before the blast wave encountered the column (i.e., while the blast was still spherical), in a multimaterial Euler wedge. When the blast shockwave was within 25 mm from the column, the results of the 2D analysis was remapped into a sphere in the three-dimensional (3D) model. This in effect sets the results of the 2D model as initial conditions for the 3D model in an ideal gas Euler mesh. The 2D blast was modeled as a multimaterial Euler wedge divided into 1975 1-mm elements and filled with air and a concentric sphere of C4. The radii of the central C4 spheres were calculated using the experimental tests' charge masses of 50 and 100 kg and the density of C4 of 1,590 kg/m³ (Unified Facilities Criteria 2002). The calculated radii for the charges were 0.196 m for the 50 kg of C4 charge and 0.247 m for the 100 kg of C4 charge.

The three components of the specimens in the 3D models were modeled distinctly rather than using a smeared approach. The concrete core was modeled using a Lagrange half cylinder, the GFRP tube was modeled as a half cylindrical shell, and the reinforcing cage was modeled using beam elements. The concrete core was meshed as a Type 2 cylinder with four elements across the radius and 80 elements along the length. The number of elements across the radius resulted in eight elements around the half circumference. These element numbers resulted in a 0.025-m cube-shaped mesh. This part was filled using the RHT model and concrete properties already discussed. The GFRP tube was divided into a grid identical to the surface of the concrete as the surface nodes of both were bonded. The tube had a thickness of 5.5 mm and was assigned the material properties of orthotropic GFRP. The longitudinal steel bars were made of continuous 2-m-long beams divided into 100 elements. These divisions satisfied *ANSYS Autodyn*'s beam element aspect ratio and ensured that every element of the concrete mesh contained a node of the beam reinforcement. This was necessary to ensure that the reinforcement forces were transmitted to the concrete when the volume reinforcement option was chosen for the beams. The continuous circular spirals were modeled using straight beam segments forming half a polygon with its vertices at the location of the longitudinal reinforcement. The spacing of the model stirrups was 0.1 m over the entire length with a reduced spacing of 0.05 m for 0.2 m from the ends over the supports to match the experimental specimens. The transverse beams were also divided into sufficient elements to ensure that there was at least one node per concrete element. The longitudinal bars were given a 100 mm² circular cross section and the 10M steel material properties, whereas the transverse bars were given a 30 mm² cross section and the 6-mm steel material properties. All the reinforcement was rigidly connected to the surrounding concrete, and no bond slip was modeled. The numerical reinforcing cages and a schematic of the experimental specimen's reinforcement cage for the two reinforcement ratios studied are shown in Fig. 2.
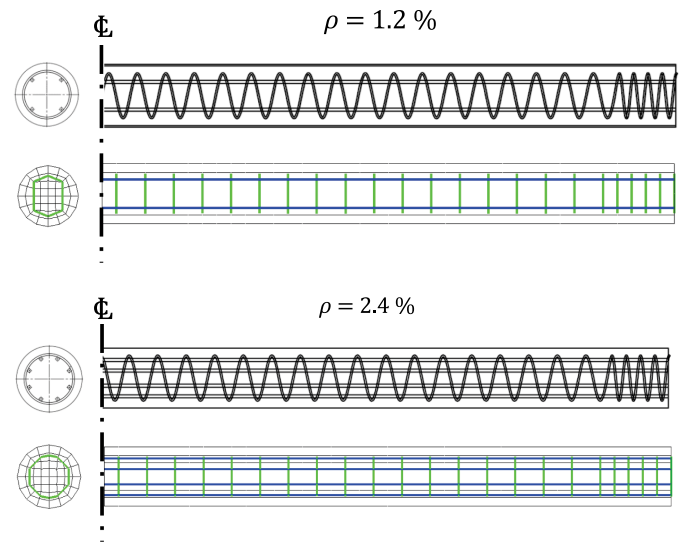

Fig. 2. Comparison of test specimens' and numerical models' reinforcement cages

The impact hammer was modeled using a prismatic rectangular Lagrange part. The dimensions of the modeled impact hammer were 0.15 m by 1.25 m by 0.075 m, and it was divided into approximately 0.035-m sided cube-shaped elements. The part was filled with *ANSYS Autodyn*'s material library's standard 4,340 Steel material with an adjusted density of 10 g · cm⁻³ to match the mass of the experimental impact hammer of 561 kg (the hammer in the model weighed 140.25 kg attributable to quarter symmetry). The modeled hammer was then given an initial velocity equal to the instantaneous velocity measured using the high-speed camera for the test being modeled. These velocities were -1.35 m · s⁻¹, -1.22 m · s⁻¹, -1.56 m · s⁻¹, and -1.32 m · s⁻¹ in the y direction for specimens CI4, CI8, TI4, and TI8, respectively. Additionally, the supports and caps were modeled using Lagrange and shell parts, respectively. The supports had a radius of 0.02 mm and were 0.1 m long. The caps were 0.15 m wide for the support and 0.075 m wide for the midspan impact cap. The caps and the supports were also filled with the modified 4340 Steel material model. A representative impact model showing the material locations is presented in Fig. 3.

The verification models' 3D Euler parts used to model the blasts and their interaction with the specimens were developed to accommodate the blast wave, the specimen length, and the influence of the approximate outflow boundary condition ($\approx$10 to 20 elements). The dimensions of the Euler 3D parts were 0.6 m in the x direction, 2.96 m in the y direction, and 2 m in the z direction. The Euler parts were divided into 10-mm cubic elements and filled with the air material. The blasts were remapped from the 2D multimaterial analysis. A representative blast model, showing the blast wave specimen interaction, is presented in Fig. 4.

Gauges and Boundaries. Because of the large number of cycles that a model will calculate before reaching the end time, *ANSYS Autodyn* will only save complete results at predetermined locations chosen by the user and referred to as numerical gauges. Such gauges were incorporated at midspan to capture the results of the models. A gauge was placed at each of the extreme fibers in tension and compression of the concrete and the tube. A gauge was also placed at each of the longitudinal bars. The blast pressure measurements on the surface of the columns were captured using two gauges, one at the point of incidence, and the other at the side
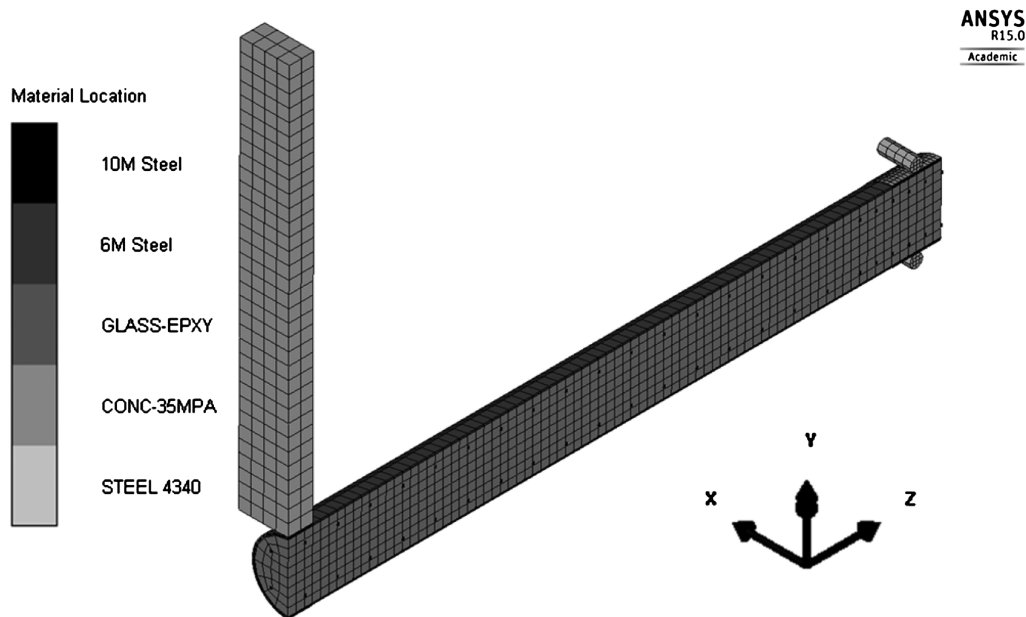
Fig. 3. Representative impact model showing material locations, sign convention, and mesh size
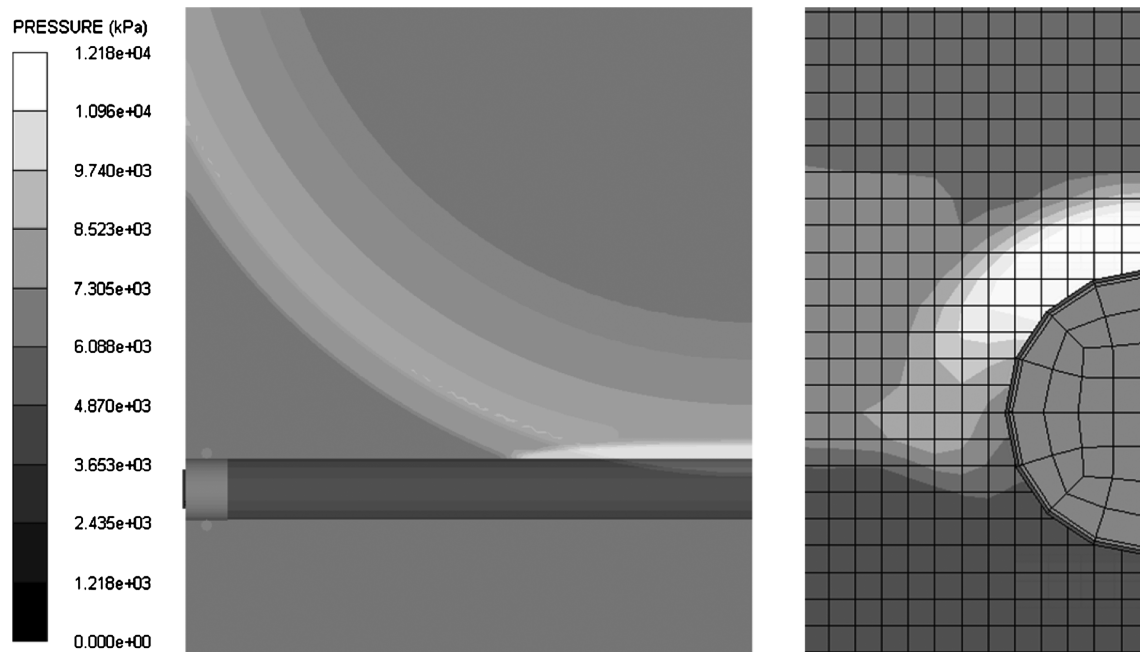

Fig. 4. Representative blast model showing Euler mesh and blast interaction with member

of the column in the Euler grid of the blast models. A gauge was placed in the hammer for the impact models.

The member's nodes on the y-z plane of symmetry were restrained from moving in the x direction. Similarly, the member's nodes in the x-y plane of symmetry were restrained from moving in the z direction. The mass was restrained from moving in both x and z directions and was not allowed to rotate. Refer to Fig. 3 for the orientation of the axis relative to the specimens. The orientation was the same for the blast and impact models. The Euler part had mirror boundaries on the planes of symmetry and the bottom, which represented the ground. The remaining three surfaces had an outflow boundary which allowed pressure and material to escape. The supports had a rigid boundary condition and were

restrained from any motion. The cap at the support was restrained from moving in the x direction. The cap at the midspan of the impact models was restrained from moving in both the x and z directions as it intersected two planes of symmetry. The gauges for a blast model with a 1.2% reinforcement ratio, the Euler part boundaries, and the axis orientation are presented in Fig. 5.

Results and Verification

Mesh Refinement

This study's mesh size was arrived at by running three models of varying mesh coarseness and comparing the results. The finest
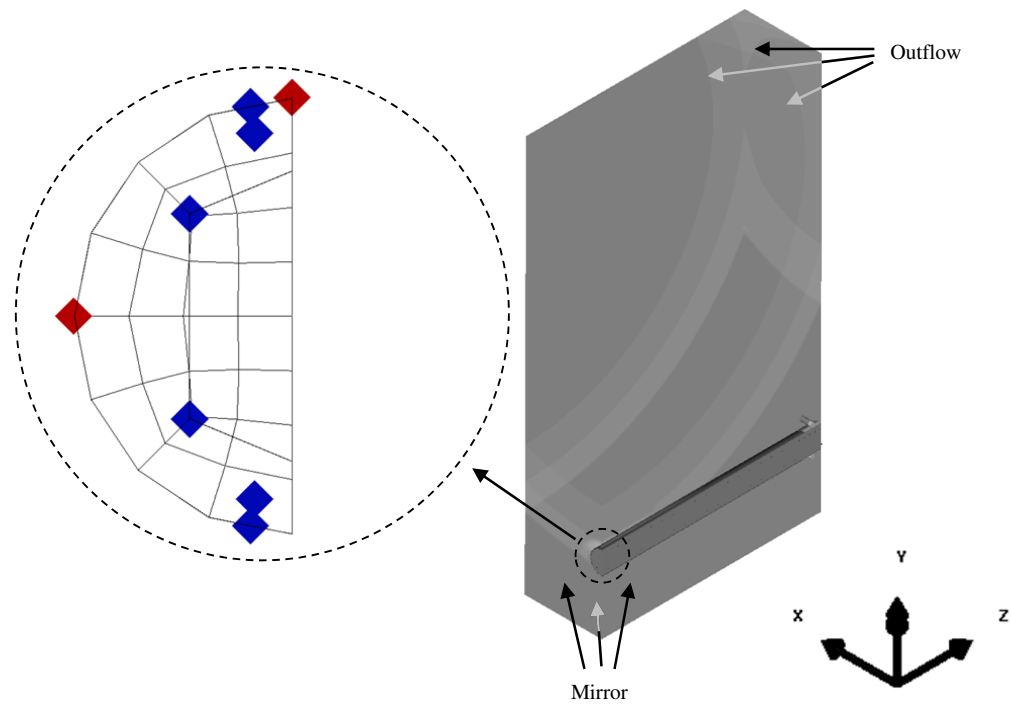
Fig. 5. Locations of gauges in impact and blast models and locations and types of boundaries in blast models

mesh divided the radius of the columns into seven elements, which resulted in 12 elements around the half circumference. The length of the specimen was divided into 130 elements resulting in 0.015-m cube-shaped elements. The reinforcement was similarly divided into 135 elements to ensure a node was located in each concrete element for the volume reinforcement option. This approached the limit of the fineness for this geometry because a finer mesh would have violated the beam elements' aspect ratio requirement of two to one. The medium coarseness mesh, the one used in this study, has already been described above. The coarsest mesh divided the radius into three elements resulting in four elements around the half circumference. The length of the column was divided into 57 elements resulting in a 0.035-m cube shaped mesh. The longitudinal beams in the extra coarse mesh were divided into 60 elements. The cross section's mesh and the numerical results of the three meshes with the experimental results are presented in Fig. 6. The three meshes produced indistinguishable results initially; however, these results diverged as the displacement increased resulting in a maximum displacement at midspan of 0.051, 0.054, and 0.061 m for the fine, medium, and coarse mesh, corresponding to a 10.9, 17.4, and 32.6% deviation from the experimental results, respectively. Thus, the variation between the fine and coarse meshes was 19.6%, and they all replicated the experimental results fairly well. The medium mesh was chosen because the coarse mesh may not have captured the interaction with the blast wave adequately, and the fine mesh was computationally prohibitive.

Impact Tests Verification

The experimental results of the impact testing phase were used to verify the numerical model prior to conducting the parametric study. These results are presented in Figs. 7(a–d). The maximum midspan displacements of the experimental results and the numerical models are summarized in Table 3. The numerical models' results matched the experimental results fairly well. In a study by Fujikake et al. (2009) on the impact behavior of reinforce

concrete beams and a second study by Han et al. (2014) on the impact behavior of concrete filled steel tubes displacement time, history analysis results were typically within 10% of the measured values for both studies. Fujikake et al. (2009), however, noted that there was a large difference between analytical and measured responses for specimens that experienced local failures in the vicinity of the impact point. All numerical displacements in this study were within 18% of experimental values. Specimen CI4 had the greatest difference of 18%, and this was attributed to the concrete crushing and spalling at the maximum displacement of this specimen which may have dissipated some of the impact's energy, resulting in a lower maximum displacement. The remaining specimens' numerical models show good agreement with experimental results and capture the maximum displacements and the periods of the specimens.
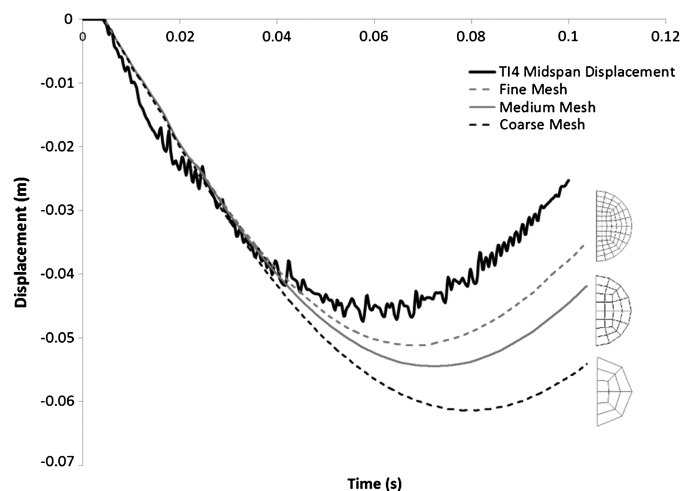

Fig. 6. Results of modeling specimen TI4 under impact using three models of varying mesh coarseness
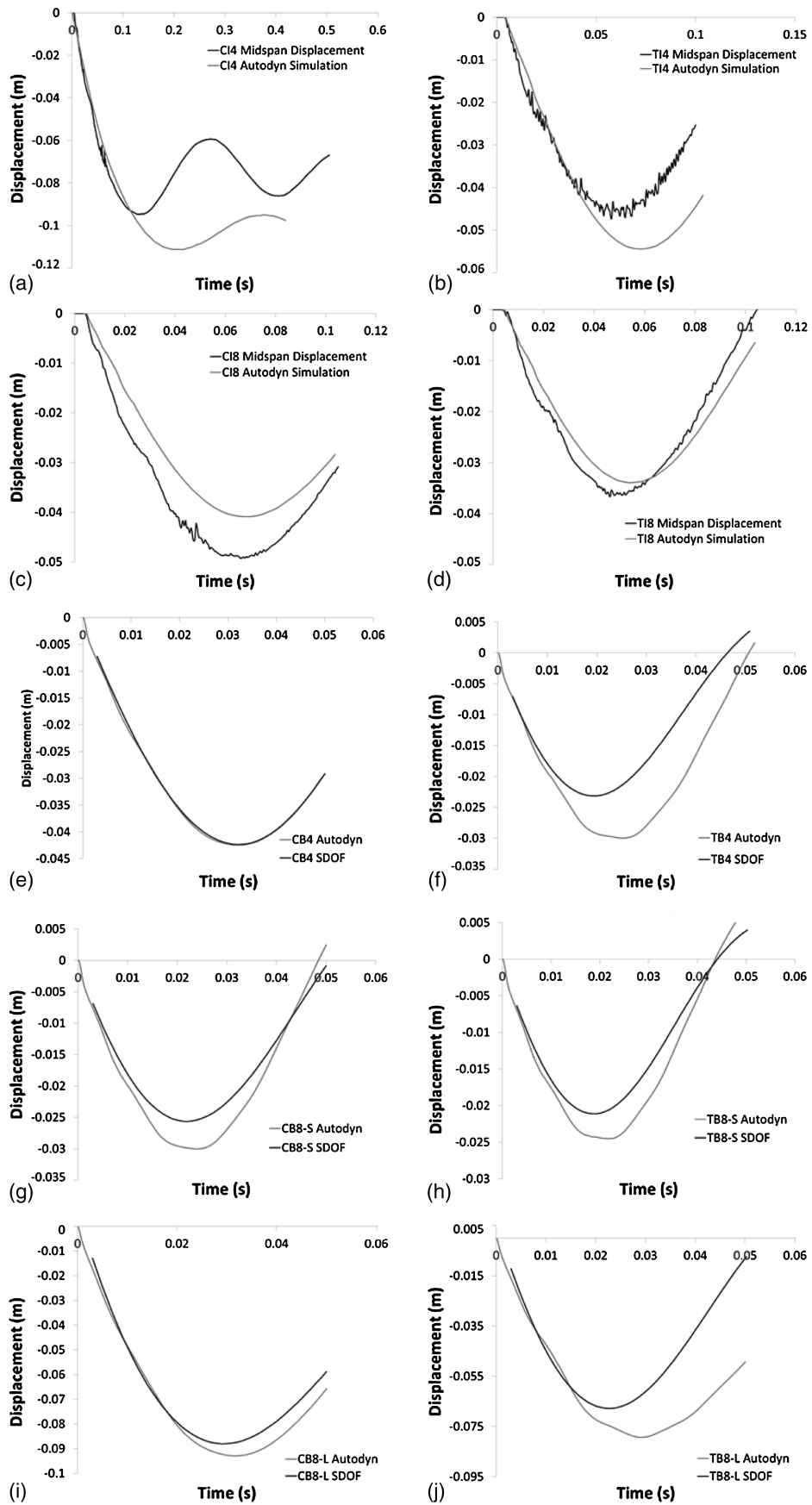
Fig. 7. (a–d) Comparison of numerical and experimental results of impact CFFT test specimens; (e–j) SDOF and numerical results for blast CFFT specimens

Table 3. Summary of Numerical Impact and Blast Model Verification Results

Specimen designation	Time to peak displacement (s)			Maximum displacement (m)		
	Experimental (impact) or SDOF (blast)	Numerical	Percentage difference	Experimental (impact) or SDOF (blast)	Numerical	Percentage difference
Impact tests						
CI4	0.130	0.209	−60.8	−0.094	−0.111	−18.1
CI8	0.065	0.069	−6.2	−0.049	−0.041	16.3
TI4	0.061	0.074	−21.3	−0.046	−0.051	−10.9
TI8	0.049	0.055	−12.2	−0.036	−0.034	5.6
Blast tests						
CB4	0.032	0.032	0.0	−0.042	−0.042	0.0
TB4	0.019	0.026	−36.8	−0.023	−0.030	−30.4
CB8-S	0.022	0.025	−13.6	−0.026	−0.030	−15.4
TB8-S	0.018	0.023	−27.8	−0.021	−0.024	−14.3
CB8-L	0.029	0.032	−10.3	−0.088	−0.093	−5.7
TB8-L	0.022	0.030	−36.4	−0.068	−0.079	−16.2

Blast Test Comparison with SDOF Results

The experimental blast tests only yielded residual displacements and visual damage to the specimens. A sophisticated single degree of freedom (SDOF) model was, however, developed to predict the behavior of the specimens in response to the blast shockwaves. The full development, verification, and results of this SDOF model have been reported elsewhere (Qasrawi 2014).

The solution of the equation of motion, given in Eq. (1), for a flexural member can be simplified to a SDOF system by assuming a shape function that is scaled by a single displacement of interest, usually the midspan displacement. An equivalent mass, damping, stiffness, and forcing function can be obtained by equating the kinetic, strain, and potential energies of the original system to those of the SDOF system

$$M_{eq}\ddot{y} + c\dot{y} + R(y) = F_{eq}(t) \tag{1}$$

where y = displacement in m; $\dot{y}$ = velocity in m · s^{-1}; $\ddot{y}$ = acceleration in m · s^{-2}; M_{eq} = equivalent mass in kg; C = damping coefficient in kg · s^{-1}; $R(y)$ = resistance as a function of displacement in N; and $F_{eq}(t)$ = loading as a function of time in N.

The complexity of the loading functions and the nonlinearity of the resistance functions made the direct solution of the differential equation of motion impossible in this case. Thus, a numerical integration approach was used (Biggs 1964).

The equivalent mass and damping were calculated using the standard procedures of equating the kinetic energies of the original and SDOF systems and logarithmic decrements of the impact tests. The complete nonlinear resistance functions for the CFFT members investigated in this paper were derived as follows. Sectional analyses were performed to obtain the moment-curvature relationships of the blast experimental test specimens. The moment-curvatures were then numerically integrated with respect to curvature to give a relationship of cross-sectional strain energy to curvature as shown in Eq. (2)

$$\frac{dU(\phi)}{dx} = \int_0^{\phi_{\max}} M(\phi)d\phi \tag{2}$$

where U = strain energy in Joules; ϕ = curvature in rad · m^{-1}; $M(\phi)$ = bending moment as a function of curvature in N · m; and x = distance along the length of a member in m.

An incrementally increasing bending moment diagram was constructed using the known loading configuration. This bending moment diagram and the moment-curvature relationship were used to find the curvature distribution along the length for the moment increment. The sectional strain energy distribution was constructed using the previously obtained strain energy to curvature relationship and the curvature distribution along the length. This in effect gave the strain energy as a function of location along the member. The displacement at the moment increment was obtained using the double integration method. The total stored strain energy of the member at the applied moment increment was obtained by numerically integrating the sectional strain energy distribution using Eq. (3)

$$U = \int_0^L \frac{dU(x)}{dx}dx \tag{3}$$

The results of these calculations were the total energy stored in the member and the corresponding displacement for the given bending moment increment. The process was then repeated for the next moment increment until the failure bending moment was reached. The result of these calculations was a relationship between the displacement of the member and the total strain energy stored in it. The derivative of this resulting strain energy versus displacement relationship was taken numerically to obtain the resistance function as shown in Eq. (4)

$$R(y) = \frac{dU(y)}{dy} \tag{4}$$

where $R(y)$ = equivalent resistance function in N.

The results of this SDOF model were used to verify the *ANSYS Autodyn* blast model. A summary of the results is presented in Table 3, and plots of the *ANSYS Autodyn* and SDOF results for the individual specimens are presented in Figs. 7(e–j). As in the case of the impact tests, the results showed good agreement and reproduced the SDOF peak displacements well. The results of specimen CB4 showed excellent agreement, whereas the results of specimen TB4 showed the largest discrepancy of 30%. The results of the remaining specimens varied by less than 16% in all cases which gave confidence in the model's ability in capturing the dynamic behavior of the CFFT system when subjected to blast loading.

Parametric Study

The parametric study investigated the effect of reinforcement ratio, diameter, and scaled distance on the response of CFFTs. The reinforcement ratios investigated were the lower and upper design limits of 1 and 2.5% (CSA 2004b; Unified Facilities Criteria 2002) and the intermediate point of 1.75%. The diameters studied were 0.2 m through to 1.0 m in increments of 0.2 m, inclusive. The blast

Table 4. Parametric Study Specimen Number and Size of Longitudinal Reinforcement

| Diameter (m) | $\rho = 1\%$ | | $\rho = 1.75\%$ | | $\rho = 2.5\%$ | |
	Number of bars	ρ (%)	Number of bars	ρ (%)	Number of bars	ρ (%)
0.2	4–10M	1.27	6–10M	1.91	8–10M	2.55
0.4	6–15M	0.95	10–15M	1.59	10–20M	2.38
0.6	10–20M	1.06	10–25M	1.77	10–30M	2.47
0.8	16–20M	0.95	14–30M	1.95	14–35M	2.78
1.0	16–25M	1.02	20–30M	1.78	20–35M	2.55

Table 5. Parametric Study's Models' Meshes and Element Divisions

Diameter (m)	Cells across radius	Cells along length	Cells around the circumference	Reinforcement divisions
0.2	4	8	8	100
0.4	5	50	8	55
0.6	5	30	8	33
0.8	6	25	12	28
1.0	7	25	12	28

scaled distances investigated were 0.2–0.5 m · kg$^{-1/3}$ in increments of 0.1 m · kg$^{-1/3}$, inclusive. These parameter ranges were arrived at as follows. The reinforcement ratios included the upper and lower limits and an intermediate point. A diameter of 0.2 m can be taken as a practical lower limit for North American concrete construction, whereas 1.0 m can be taken to represent an upper limit. The lower bound of the scaled distance of 0.5 m · kg$^{-1/3}$ was similar to the scaled distances studied in the experimental investigation, which produced minimal damage. The upper bound was dictated by geometric considerations of the numerical models.

The models' lengths were held constant at 2 m, which corresponded to a specimen length of 4 m. This was to avoid introducing an additional parameter to the study. The specimens' longitudinal reinforcement ratio was approximated using standard metric reinforcing bars, as presented in Table 4. Extra care was taken in choosing the bar sizes to ensure a realistic and uncongested reinforcement arrangement. All the specimens contained 6-mm ties spaced at 0.1 m except for one diameter length over the supports, where the spacing was reduced to 0.05 m to counteract the effect of the concentrated reactions. The scaled distances of the parametric study were achieved using TNT rather than C4 because TNT is the standard explosive and no conversions would be necessary. The study's scaled distances ranged from 0.2 to 0.5 m · kg$^{-1/3}$ in increments of 0.1 m · kg$^{-1/3}$ corresponding to charge masses of 1,000, 296, 125, and 64 kg and radii of 0.527, 0.351, 0.264, and 0.211 m, respectively. The radii were calculated from the masses using the TNT density of 1,630 kg · m^{-3} (Unified Facilities Criteria 2002). The parametric study's blasts were initially modeled using 2D axis symmetry from the explosion out to 1.999 m in a multimaterial Euler wedge divided into 1999 1-mm wide elements and filled with air and a concentric TNT sphere.

The parametric study's concrete core mesh sizes were arrived at by satisfying the 2.5% reinforcement ratio's models reinforcement aspect ratio requirements. All the concrete cores were meshed as Type 2 half cylinders with the mesh details presented in Table 5. These parts were filled with the RHT model and a 35-MPa concrete compressive strength. The shell modeling the GFRP tube was divided into a grid corresponding to the cells along the length and cells around the circumference presented in Table 5. The shell was bonded to the concrete core. The tube thickness of 5.5 mm and the orthotropic GFRP material properties were not altered. The longitudinal steel bars' divisions, presented in Table 5, satisfied *ANSYS Autodyn*'s beam element aspect ratio requirement and ensured that every element of the concrete mesh contained a node of
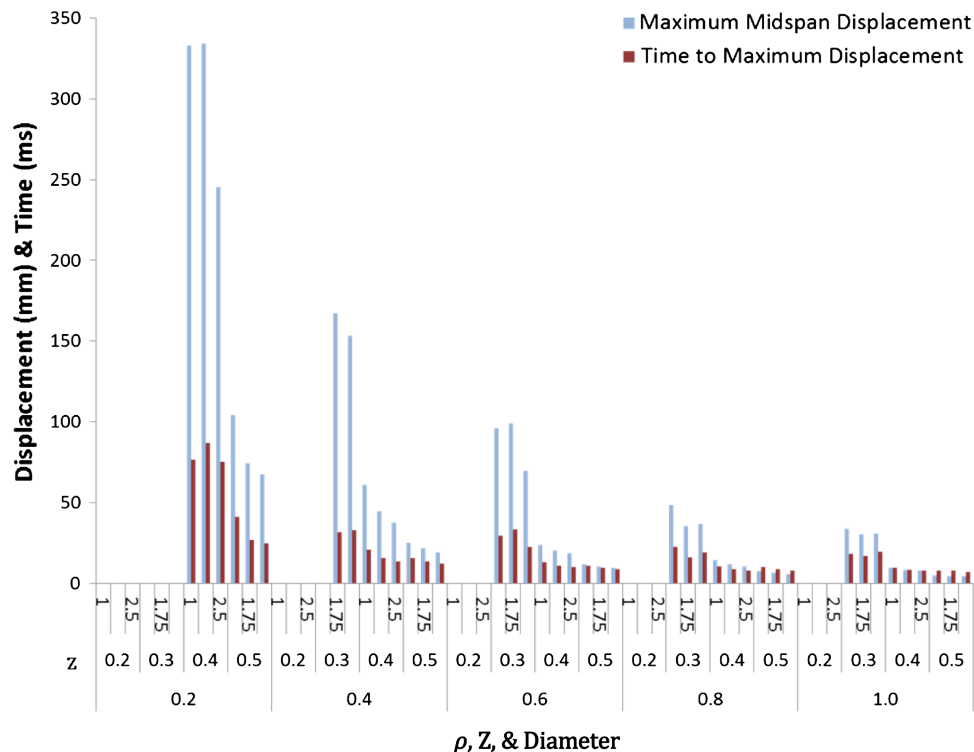
Fig. 8. Maximum displacements and times to peak results of parametric study

the beam reinforcement. The shear reinforcement was modeled using straight beam segments forming half a polygon with its vertices at the location of the longitudinal reinforcement. The spacing of the model stirrups was 0.1 m over the entire length with a reduced spacing of 0.05 m for one-diameter length over the supports to mitigate the effect of the concentrated loads. The transverse beams were also divided into sufficient elements to ensure that there was at least one node per concrete element. The longitudinal bars were assigned the section properties presented in Table 4 and the 10M steel material properties, whereas the transverse bars were given a 30 mm^2 cross section and the 6-mm steel material properties. The supports and cap were modeled using Lagrange and shell elements. The supports had a radius of 0.02 mm and were 0.1 m long. The cap was 0.15 m wide. The caps and the supports were filled with the 4340 Steel material model with the slightly modified density of 10 g · cm^{-3}. The caps' thicknesses were varied from 5 to 25 mm in increments of 5 mm, for the 0.2 m to 1.0 m diameter models, respectively, to accommodate the increasing support reactions for the larger diameters.

It was necessary to use multimaterial 3D Euler parts to model the blasts because of their close-in nature. The following guidelines were followed while building the parametric study's 3D Euler parts. The dimensions of the Euler parts were dictated by the 2 m range of the blast, the column diameter, the model length, and the influence of the approximate outflow boundary condition ($\approx$10 to 20 elements). Therefore, the dimensions of the Euler parts were the radius plus 0.5 m in the x direction, the diameter plus 0.5 m below and 2 m above the specimen in the y direction, and 2 m in the z direction. The Euler part was divided into 0.02-m cubic elements and filled with the air material. The blasts were remapped from a 2D multimaterial analysis. The gauges and boundaries were the same as the verification models except that the blast exited through an outflow boundary at the bottom of the model as opposed to being reflected back up to replicate the experimental situation.

Parametric Results

The overall results of the parametric study are presented in Fig. 8 for the maximum displacements and times to peak. Each column in the figure represents the maximum displacement or time to peak for a single numerical model. The results are organized in a hierarchy starting with the diameter, followed by the scaled distance, then the reinforcement ratio. The gaps in the diagram represent models that collapsed under the blast loading. All the models collapsed under a scaled distance of 0.2 m · kg$^{-1/3}$. Additionally, all the 0.2-m diameter models and the 0.4-m diameter model with a reinforcement ratio of 1% collapsed under a scaled distance of 0.3 m · kg$^{-1/3}$. The following general trends can be observed. For a given scaled distance in Fig. 8, the maximum achieved midspan displacement decreased as the diameter was increased. This relationship, however, was not linear and seemed to be an exponential decay. A similar exponential decay relationship was observed for a given diameter as the scaled distance was increased. This relationship holds for all reinforcement ratios. The time to peak, which was proportional to the natural period of the beams, behaved slightly differently. It was fairly constant for the larger scaled distances, whereas it increased with decreasing scaled distance. This can be explained by the inversely proportional relationship of the natural period to stiffness. As the scaled distance decreased, the damage produced in the model increased, thus decreasing its stiffness. This in turn caused the period to increase.

Inspecting Fig. 8 also revealed that for a scaled distance of 0.3 m · kg$^{-1/3}$, the trends were inconsistent, and the models with a larger reinforcement ratio, which determined strength and stiffness, in some cases reached a higher maximum displacement for a given diameter. This was attributable to some of the weaker models developing a plastic hinge at the support owing to direct shear and responding in either direct shear or a combination of direct shear and flexure. Direct, or dynamic, shear is a response typical for short duration high intensity loads and typically occurs at locations of geometric or load discontinuity. It arises from the large inertial forces developed early on in the loading (Nystrom 2008). Although direct shear was a local response, typically occurring near the supports, it affected the global response of the entire member, as demonstrated from the results. Two 0.4-m-diameter models at their peak displacements are presented in Fig. 9. The figure shows the overall member's deformed shape and the stresses in the steel reinforcement. The flexural response mode's stress distribution was typical and showed large compressive and tensile stresses at the top and bottom layers of rebar at midspan, respectively, whereas the stresses were relatively low in the shear reinforcement. The direct shear response mode showed a similar longitudinal reinforcement stress distribution to the flexural response mode, indicating a combined flexural and direct shear response. In addition to the
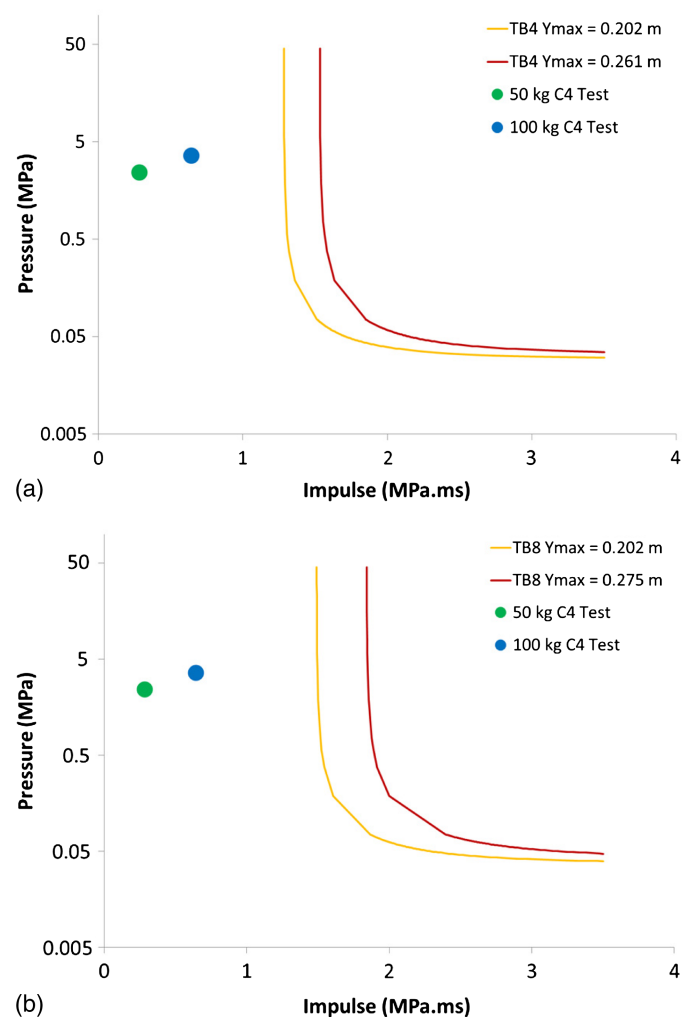

Fig. 9. Flexural and direct shear response of 0.4-m diameter model subjected to two different magnitude blasts
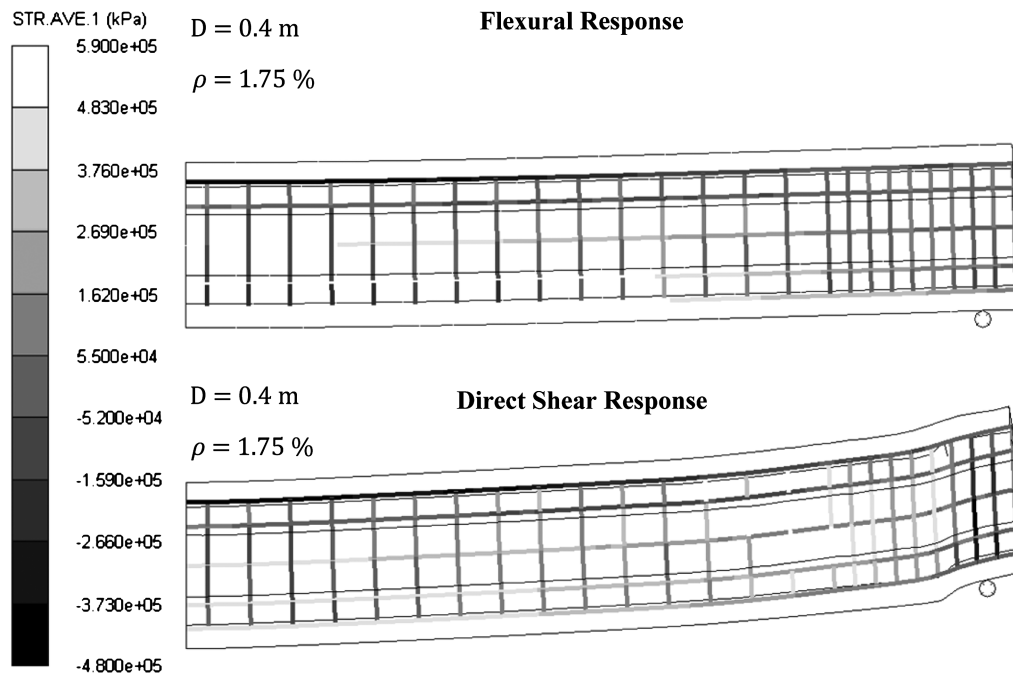
Fig. 10. Pressure-impulse diagrams for specimens TB4 and TB8

flexural stresses, however, large stresses developed in the transverse reinforcement near the support. The tube typically ruptured near the supports in the direct shear response models attributable to the large localized strains that developed.

The UFC 3-340-01 (Unified Facilities Criteria 2002) specified the maximum response limit for a simply supported reinforced concrete member as a maximum support rotation of 0.105 rad (6°), which translated to a midspan displacement of 0.211 m, assuming a plastic hinge formed at midspan. All the 0.2-m-diameter specimens subjected to a scaled distance of 0.4 m · kg$^{-1/3}$ exceeded this limit and survived, with the 2.5% reinforcement ratio specimen undergoing a 0.245-m maximum displacement, corresponding to an end rotation of 0.1225 rad (7°), whereas the 1.75 and 1% models experienced a maximum displacement of 0.333 m each, corresponding to a 0.165 rad (9.45°) support rotation. It is worth noting that the response limit for moderate damage of a restrained member is 0.21 rad (20°), and that two of the specimens have sustained 79% of that limit. This new insight into the behavior of CFFTs under blast loading can be applied to the experimental results discussed elsewhere (Qasrawi 2014). Thus, the pressure-impulse (P-I) diagrams can be extended beyond the limit recommended by the UFC 3-340-01 (Unified Facilities Criteria 2002). The new midspan displacement limits were taken as the maximum displacement of the resistance functions derived in the blast elsewhere (Qasrawi 2014) because the tube ruptured in the numerical models that

reached a displacement of 0.333 m. Those limits were 0.261 m for TB4 and 0.275 m for TB8. The resulting P-I diagrams, including the experimental blast tests, are presented in Fig. 10(a) for specimen TB4 and in Fig. 10(b) for specimen TB8, and the values of the asymptotes used in the diagrams are presented in Table 6. Increasing the allowable midspan displacement increased the strain energy available to resist a blast by 43% for specimen TB4, which had a steel reinforcement ratio of 1.2%, and 52% for specimen TB8, which had a steel reinforcement ratio of 2.4%. These increases in the available strain energies translated to a 15 and 17% increase in the pressure and impulse, respectively, that specimen TB4 was able to withstand, and a 23 and 24% increase in the pressure and impulse, respectively, that specimen TB8 was able to withstand. Although none of the models was considered a deep flexural beam according to the UFC 3-340-01 (Unified Facilities Criteria 2002) unrestrained member criterion of $L/h \leq 2$; it is easy to see that the deeper a member was, the less ductile it was. That is because for a given curvature, which can be thought of as the slope of the strain distribution across the depth, the strains developed at the extreme fibers were proportional to the depth of the section. This led to achieving the failure strain at a lower curvature, leading to a lower overall deformation.

The overall pressure results of the parametric study, presented in Fig. 11, supported the conclusions arrived at in another study (Qasrawi et al. 2015), that the reflected pressure experienced by a member with a circular cross section for a given scaled distance was proportional to the diameter, and that this pressure approached the design value as the diameter was increased. The incident pressure recorded at the side of the column, on the other hand, decreased with increasing diameter as expected, as the shock wave had to travel a longer distance and dissipated more energy. Inspecting the details of the diagram revealed that the reflected pressure was not affected by the stiffness of the model as the reflected pressure was fairly constant for the range of reinforcement ratios studied. Similar observations can be made regarding the impulse presented in Fig. 12.

Table 6. Asymptotes of Updated P-I Diagrams for Specimens TB4 and TB8

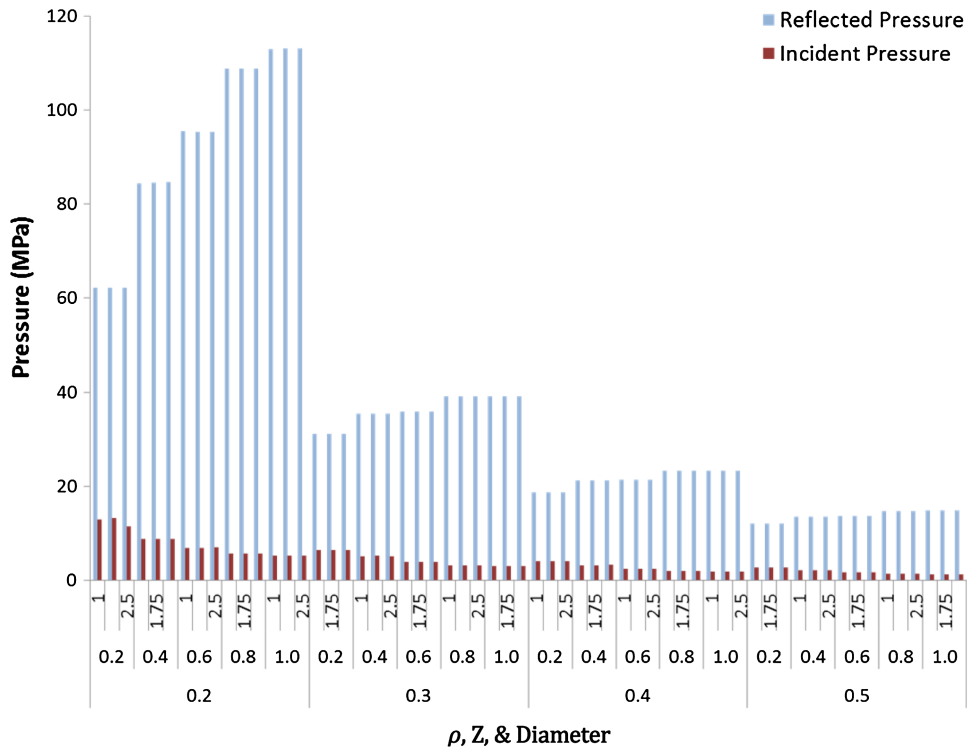| Specimen	Ymax (m)	Strain energy (J)	Force (N)	Impulse (N · s)	Pressure (MPa)	Impulse (MPa · ms)
TB4	0.202	8,060	40,300	1,723	0.031	0.131
	0.261	11,504	46,500	2,023	0.035	1.533
TB8	0.202	10,163	50,815	1,967	0.039	1.500
	0.275	15,491	62,500	2,430	0.047	1.841

© ASCE

J. Struct. Eng.

Fig. 11. Overview of reflected pressure and incident pressure parametric study results
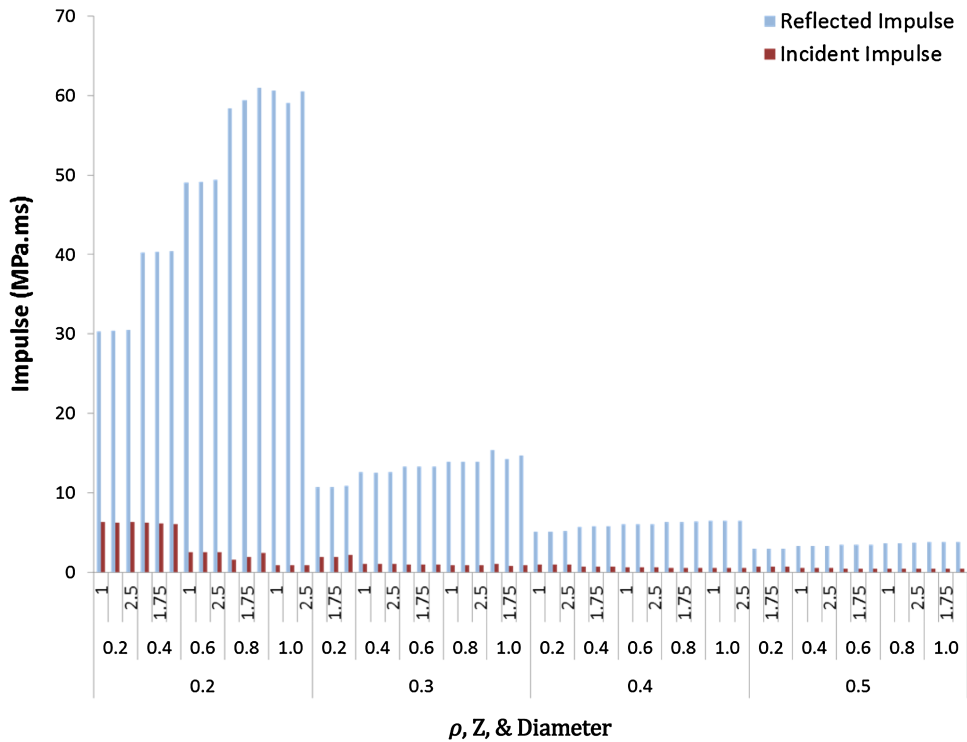

Fig. 12. Overview of reflected impulse and incident impulse parametric study results

Conclusion

FRP has been demonstrated experimentally to improve a structural member's strength and stiffness and is promising for blast resistant applications. However, design guidelines need to be developed for the use of FRP in these applications. A practical way to supplement the limited amount of experimental blast data to develop design guidelines is through numerical modeling.

This paper has demonstrated the feasibility of using the commercially available software *ANSYS Autodyn* to predict the

response of CFFTs to close-in blast and impact loading. The numerical models were able to capture the large variability and complex interactions between a blast wave and a CFFT member.

The model was validated using experimental results of full-scale CFFT blast and impact tests. The model's peak deflection results were typically within 16% of the experimental results, which is similar to what other researchers have reported in the literature. This gave confidence in the model's ability to capture the dynamic behavior of CFFTs under blast loading. The model was then used to conduct a parametric study of the behavior of CFFTs subjected to blast loading. The aim of the parametric study was to establish the effects of the diameter, scaled distance, and reinforcement ratio on the response of CFFTs to close-in blast loading. The results of the parametric study indicated that increasing the diameter or the reinforcement ratio reduced the overall response to the blast for a given scaled distance. Alternatively, reducing the scaled distance increased the midspan deflection for a given member diameter and reinforcement ratio. Based on the results of this parametric study, it is recommended that the maximum allowable displacement be increased from 0.211 to 0.261 m for CFFTs to account for their additional energy absorbing capability. The parametric study also supported the pressure impulse distributions around circular cross sections arrived at in a previous study.

Acknowledgments

References

ANSYS Autodyn. (2005). "Theory manual revision 4.3." Century Dynamics, Concord, CA.

Ameron International. (1997). "Series 5000 fiberglass pipe and fittings: For severely corrosive industrial service." Bondstrand Product Data, Houston.

Ameron International. (2004). "Caesar II allowable stress input for UKOOA code." Houston.

Barker, D. D. (2008). "Advanced analysis topics for blast resistant buildings in petrochemical facilities." *ASCE Structures Congress 2008*, ASCE, Reston, VA, 1–4.

Bazant, Z. P., and Becq-Giraudon, E. (2002). "Statistical prediction of fracture parameters of concrete and implications for choice of testing standard." *Cem. Concr. Res.*, 32(4), 529–556.

Biggs, J. (1964). *Introduction to structural dynamics*, McGraw-Hill, New York.

Buchan, P. A., and Chen, J. F. (2007). "Blast resistance of FRP composites and polymer strengthened concrete and masonry structures—A state-of-the-art review." *Compos. Part B*, 38(5-6), 509–522.

Cole, B., and Fam, A. (2006). "Flexural load testing of concrete-filled FRP tubes with longitudinal steel and FRP rebar." *J. Compos. Constr.*, 10.1061/(ASCE)1090-0268(2006)10:2(161), 161–171.

CSA (Canadian Standards Association). (2004a). "Compressive strength of cylindrical concrete specimens." *A23.2-9 C*, Mississauga, ON, Canada.

CSA (Canadian Standards Association). (2004b). "Design of concrete structures." *A23.3-04*, Mississauga, ON, Canada.

Elgawady, M., Booker, A., and Dawood, H. (2010). "Seismic behavior of posttensioned concrete-filled fiber tubes." *J. Compos. Constr.*, 10.1061/(ASCE)CC.1943-5614.0000107, 616–628.

Fam, A., and Mandal, S. (2006). "Prestressed concrete-filled fiber-reinforced polymer circular tubes tested in flexure." *PCI J.*, 51(4), 42–54.

Fam, A., and Rizkalla, S. (2002). "Flexural behavior of concrete-filled fiber-reinforced polymer circular tubes." *J. Compos. Constr.*, 10.1061/(ASCE)1090-0268(2002)6:2(123), 123–132.

Flisak, B., Fam, A., and Rizkalla, S. (2001). "FRP tubes filled with concrete and subjected to combined axial and flexural loads." *Construction Institute Sessions at ASCE Civil Engineering Conf.*, ASCE, Reston, VA.

Fujikake, K., Li, B., and Soeun, S. (2009). "Impact response of reinforced concrete beam and its analytical evaluation." *J. Struct. Eng.*, 10.1061/(ASCE)ST.1943-541X.0000039, 938–950.

Han, L.-H., Hou, C.-C., Zhao, X.-L., and Rasmussen, K. J. (2014). "Behaviour of high-strength concrete filled steel tubes under transverse impact loading." *J. Constr. Steel Res.*, 92, 25–39.

Helmi, K., Fam, A., and Mufti, A. (2008). "Fatigue life assessment and static testing of structural GFRP tubes based on coupon tests." *J. Compos. Constr.*, 10.1061/(ASCE)1090-0268(2008)12:2(212), 212–223.

Johnson, G. R., and Cook, W. H. (1983). "A constitutive model and data for metals subjected to large strain, high strain rates and high temperatures." *Proc., 7th Int. Symp. on Ballistics*, Hague, Netherlands, 541–547.

Luccioni, B. M., Ambrosini, R. D., and Danesi, R. F. (2004). "Analysis of building collapse under blast loads." *Eng. Struct.*, 26(1), 63–71.

Malvar, L. J., Crawford, J. E., and Morrill, K. B. (2007). "Use of composites to resist blast." *J. Compos. Constr.*, 10.1061/(ASCE)1090-0268(2007)11:6(601), 601–610.

Nystrom, U. (2008). "Concrete structures subjected to blast and fragment impacts: Numerical simulations of reinforced and fibre-reinforced concrete." Chalmers Univ. of Technology, Goteborg, Sweden.

Qasrawi, Y. (2014). "The dynamic response of concrete filled FRP tubes subjected to blast and impact loading." Ph.D. thesis, Queen's Univ., Kingston, ON, Canada.

Qasrawi, Y., Heffernan, P. J., and Fam, A. (2015). "Numerical determination of reflected blast parameters acting on circular cross sections." *Int. J. Protective Struct.*, 6(1), 1–22.

Riedel, W., Thoma, K., Hiermaier, S., and Schmolinske, E. (1999). "Penetration of reinforced concrete by BETA-B-500, numerical analysis using a new macroscopic concrete model for hydrocodes." *Proc., (CD-ROM) 9. Int. Symp. on the Interaction of the Effects of Munitions with Structures*, Berlin.

Unified Facilities Criteria. (2002). "Design and analysis of hardened structures to conventional weapons effects." *UFC 3-340-01*, U.S. Dept. of Defense, Washington, DC.

Zaghi, A. E., Saiidi, M. S., and Mirmiran, A. (2012). "Shake table response and analysis of a concrete-filled FRP tube bridge column." *Compos. Struct.*, 94(5), 1564–1574.

Zakaib, S. E. (2013). "Flexural performance and moment connections of concrete-filled GFRP tubes (CFFTS) and CFFT-encased steel I-sections." Master's thesis, Queen's Univ., Kingston, ON, Canada.